

Dependence on the initial conditions of scalar mixing in the turbulent wake of a circular cylinder

Cite as: Physics of Fluids 16, 3161 (2004); <https://doi.org/10.1063/1.1766033>

Submitted: 23 July 2003 . Accepted: 05 May 2004 . Published Online: 07 July 2004

S. Beaulac, and L. Mydlarski



View Online



Export Citation

ARTICLES YOU MAY BE INTERESTED IN

[Simultaneous velocity-temperature measurements in the heated wake of a cylinder with implications for the modeling of turbulent passive scalars](#)

Physics of Fluids **23**, 055107 (2011); <https://doi.org/10.1063/1.3586802>

[A numerical investigation on the effect of the inflow conditions on the self-similar region of a round jet](#)

Physics of Fluids **10**, 899 (1998); <https://doi.org/10.1063/1.869626>

[Small scale turbulence and the finite Reynolds number effect](#)

Physics of Fluids **29**, 020715 (2017); <https://doi.org/10.1063/1.4974323>

Physics of Fluids

SPECIAL TOPIC: Flow and Acoustics of Unmanned Vehicles

Submit Today!



Dependence on the initial conditions of scalar mixing in the turbulent wake of a circular cylinder

S. Beaulac and L. Mydlarski

Department of Mechanical Engineering, McGill University, 817 Sherbrooke Street West, Montréal, Québec H3A 2K6, Canada

(Received 23 July 2003; accepted 5 May 2004; published online 7 July 2004)

The effect of the initial conditions on scalar mixing in the turbulent wake of a circular cylinder is studied. The scalar under consideration is temperature and it is injected by means of an array of parallel, heated, fine wires (a mandoline). The initial length scale of the velocity field is varied (relative to that of the scalar field) by changing the downstream location of the mandoline. The initial length scale of the scalar field is modified by changing the number of mandoline wires and their spacing. In accordance with previous results in homogeneous, isotropic, grid turbulence, increasing the initial length scale of the velocity field was found to (i) increase the decay rate of scalar variance (m), (ii) decrease the integral scale of the scalar field (ℓ_θ), and (iii) increase the mechanical to thermal time scale ratio r . Varying the mandoline wire spacing had little effect on m , ℓ_θ , or r . Increasing the width of the mandoline decreased the scalar variance decay rate. Doing so, however, had negligible effect on the structure of the scalar field (i.e., ℓ_θ or r). The independence of the scalar variance decay rate and the structure of the scalar field—the opposite of what is observed in grid turbulence—is attributed to the inhomogeneous nature of the flow. © 2004 American Institute of Physics. [DOI: 10.1063/1.1766033]

I. INTRODUCTION

The mixing of scalars (e.g., temperature, moisture, chemical species/pollutant concentration, etc.) in turbulent flows underlies a variety of phenomena, including atmospheric and oceanic science, pollutant dispersion and combustion.^{1,2} A thorough understanding of the turbulent scalar field is therefore required to accurately predict the transport and mixing of scalars in industrial and environmental processes. To this end, it is of interest to study how a turbulent velocity field uniformizes an initially nonuniform scalar field. This process is not trivial because (i) our understanding of the velocity field remains incomplete and (ii) the coupling of the scalar and velocity fields is still unclear. The present work serves to elucidate the latter.

The most fundamental studies of the decay of scalar fluctuations in a turbulent flow were performed in homogeneous, isotropic, grid-generated turbulence.^{3–10} (In most cases, the fluid under consideration was air and the scalar was temperature.^{3–5,7–10}) In such experiments, the decay of the (passive) scalar variance is of particular interest and previous research has shown that it follows a power law:

$$\frac{\langle \theta^2 \rangle}{T_{ref}^2} = A \left(\frac{x - x_{o_\theta}}{M} \right)^{-m}, \quad (1)$$

where $\langle \theta^2 \rangle$ is the variance of the scalar fluctuations, T_{ref} is a mean reference value of the scalar, x is the distance downstream of the grid, x_{o_θ} is a virtual origin for the scalar field (assumed to be 0 in many works), and M is the grid mesh size. A and m are constants for a given set of experimental

conditions and angular brackets denote averages. The decay of the turbulent kinetic energy in grid turbulence is also given by a power law:

$$\frac{\langle u_i u_i \rangle}{U_{ref}^2} = B \left(\frac{x - x_o}{M} \right)^{-n}. \quad (2)$$

u_i represents the velocity fluctuation and U_{ref} is the mean (longitudinal) velocity of the flow. B and n are constants. x_o is the virtual origin for the velocity field.

The decay exponent of the scalar (m) has been shown to vary greatly (i.e., from 0.87 to 3.1). (See Fig. 1 of Warhaft and Lumley⁹ for a summary of scalar variance decay laws from different experiments.) This variation is significantly larger than that of n , which has been shown to vary from 1.15 to 1.45 in grid turbulence, with most of the data being consistent with $n \approx 1.3$.¹¹ From these results, it can be inferred that the ratio m/n is nonunique.

For the particular case of homogeneous, isotropic, grid-generated turbulence, the definition of the mechanical to thermal time scale ratio r ,

$$r = \frac{\tau}{\tau_\theta} = \frac{\langle u_i u_i \rangle / \epsilon}{\langle \theta^2 \rangle / \epsilon_\theta}, \quad (3)$$

reduces to $r = m/n$ using Eqs. (1) and (2), and the budgets of turbulent kinetic energy and scalar variance, respectively:

$$\frac{1}{2} \frac{d\langle u_i u_i \rangle}{dt} = -\epsilon \quad (4)$$

and

$$\frac{1}{2} \frac{d\langle \theta^2 \rangle}{dt} = -\epsilon_\theta. \quad (5)$$

τ is the mechanical time scale, τ_θ is the thermal time scale, $1/2\langle u_i u_i \rangle$ is the turbulent kinetic energy per unit mass, $\epsilon \equiv (v/2)\langle (\partial u_i/\partial x_j + \partial u_j/\partial x_i)(\partial u_i/\partial x_j + \partial u_j/\partial x_i) \rangle$ is the dissipation rate of turbulent kinetic energy, and $\epsilon_\theta \equiv \kappa\langle (\partial \theta/\partial x_i)^2 \rangle$ is the rate at which scalar fluctuations are “smeared” by molecular effects. In this work, the latter two are, respectively, estimated (assuming local isotropy and invoking Taylor’s hypothesis) by $\epsilon = 15\nu/U^2\langle (\partial u/\partial t)^2 \rangle$ and $\epsilon_\theta = 3\kappa/U^2\langle (\partial \theta/\partial t)^2 \rangle$. Given that m/n is nonunique, so too will be the mechanical to thermal time scale ratio r . The variation in r was investigated by Warhaft and Lumley,⁹ Sreenivasan, Tavoularis, Henry, and Corrsin,¹⁰ and Durbin.¹² It is of particular importance to turbulence modeling given that r is a relevant parameter in second-order turbulence models and mixing models in probability density function methods (see, for example, Refs. 13–15).

Warhaft and Lumley⁹ (herein referred to as W&L) performed two sets of experiments that studied the decay of (passive) temperature fluctuations in grid-generated turbulence. In the first set, the scalar (temperature) was injected into the turbulence by heating the grid. W&L showed that the decay rate of the passive temperature fluctuations generated in this way was a function of the initial temperature fluctuation intensity (i.e., a function of the heating applied to the grid). The implication is that “varying the temperature of the grid might vary the geometry of the thermal field.”⁹ In the second set of experiments, using an array of fine, parallel, heated wires (called a *mandoline*), they were able to generate temperature fluctuations with (i) a decay rate that was independent of their initial intensity and (ii) an initial scale that could be controlled independently of that of the velocity field. By varying the position of the mandoline downstream of the grid and the spacing between the mandoline wires, W&L were able to observe significant changes in the decay exponent m (from 1.29 to 3.20), implying a nonunique value of m/n . W&L concluded that the decay rate of the temperature fluctuations (when generated by a mandoline) is a function of the characteristic length of the temperature field, with faster decay rates being related to smaller scales. In particular, they observed an approximately linear dependence between m and k_{\max} , where k_{\max} is the wavenumber corresponding to the peak of the three-dimensional temperature spectrum. (k_{\max}^{-1} can be considered a characteristic length of the scalar field.)

Sreenivasan, Tavoularis, Henry, and Corrsin¹⁰ (herein referred to as STH&C) performed similar experiments to those of W&L. In grid turbulence, they generated isotropic, passive thermal fields with scales larger than or equal to the grid mesh size by heating the bars of the grid. They also generated passive temperature fluctuations on scales smaller than the grid mesh size by means of a mandoline. (Like with the work of W&L, the latter mandoline experiments—where the scalar field is generated independently from the velocity field—are more relevant to the present work.) STH&C found the decay exponent m to be independent of the mandoline wire spacing, the initial intensity of the fluctuations, and

mandoline downstream location (over the range of wire spacings and downstream locations considered).

The difference in the conclusions of W&L and those of STH&C was explained by Durbin.¹² It stems from the fact that in W&L, $M/M_\theta \leq 1$ whereas in STH&C, $M/M_\theta > 1$. (M is the mesh spacing of the turbulence generating grids and M_θ is the mandoline wire spacing. M characterizes the scale of the velocity fluctuations, while M_θ characterizes that of the scalar field.) Using his Lagrangian dispersion theory,¹⁶ Durbin demonstrated that m depends on the ratio of the initial length scales of velocity and temperature. For large enough values of this ratio, Durbin¹² showed that the dependence of m on it becomes negligible. The experiments of STH&C fell within this range, whereas those of W&L did not.

The principal objective of this work is to extend the results of Warhaft and Lumley⁹ and Sreenivasan, Tavoularis, Henry, and Corrsin¹⁰ to an inhomogeneous flow, viz., the wake of a circular cylinder. The scalar variance budget in a heated wake is given by

$$\frac{1}{2} \frac{d\langle \theta^2 \rangle}{dt} + \frac{1}{2} \frac{\partial \langle v \theta^2 \rangle}{\partial y} + \langle v \theta \rangle \frac{\partial T}{\partial y} = -\epsilon_\theta. \quad (6)$$

It is clearly more complex than in homogeneous, isotropic turbulence due to the presence of turbulent transport and production of scalar variance.

A significant amount of research has been undertaken in homogeneous, isotropic turbulence (e.g., Refs. 17–29). However, the scalar mixing process—especially the downstream evolution of the scalar variance and its dependence on initial conditions—in inhomogeneous flows has received much less attention (e.g., Refs. 30 and 31) and is the focus of this work.

The traditional method of generating a wake with temperature fluctuations has been to heat (usually electrically) the cylinder itself (e.g., Refs. 32–38). Beaulac³⁹ also performed experiments using a heated cylinder, but these results are not presented herein. Such a method does not permit an independent variation of the initial length scale of the velocity and scalar fields, and is analogous to heated-grid-turbulence experiments. The use of a mandoline, however, eliminates this limitation. Mandolines have been employed by previous researchers to generate scalar fluctuations in the wake of a cylinder,^{40,41} but their work only studied scaling laws in a heated wake for one mandoline configuration and did not examine the effect of different scalar field initial conditions.

The remainder of this paper is organized as follows. The apparatus is described in Sec. II. In Sec. III, the characteristics of the velocity and thermal fields are established. The results are presented in Sec. IV, where they are divided according to (i) the effect of the velocity integral scale on the scalar field and (ii) the effect of the scalar injection scale on the scalar field. A discussion of the results is given in Sec. V and the conclusions are presented in Sec. VI.

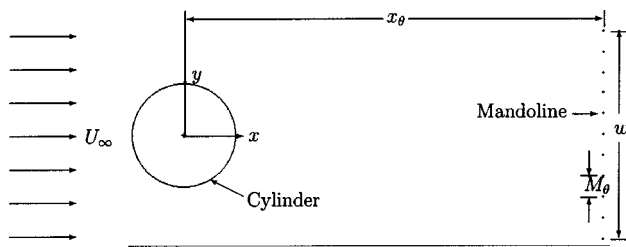


FIG. 1. Physical parameters used to specify a mandoline configuration.

II. APPARATUS

The experiments were conducted in the $0.853 \times 1.22 \times 2.74 \text{ m}^3$, low-background-turbulence wind tunnel, located in the Aerodynamics Laboratory at McGill University. The wind tunnel is of a standard open-circuit, suction design. The entrance to its plenum chamber begins with aluminum honeycomb (of 6.35 mm cell size and 152 mm long). The honeycomb is followed by four screens of stainless steel wire mesh (with a wire diameter of 0.229 mm and a mesh size of 1.27 mm). An ~ 9 -to-1 area ratio contraction following a fifth-order polynomial profile joins the plenum section ($2.87 \times 3.23 \text{ m}^2$) to the test section ($0.853 \times 1.22 \text{ m}^2$). The test section has beveled corners that slowly decrease in size in the downstream direction (resulting in an increasing cross-sectional area) to maintain a zero-pressure-gradient flow. A 8.84 m long small-angle diffuser connects the test section to a 2.13 m diameter axial fan. The rotational speed of the fan is controlled by a Unico controller to within ± 1 rpm, ensuring the stability of the mean flow. The fan is driven by a 125 hp AC motor. The experiments described herein were conducted at a free-stream velocity of 10.2 m/s. At this speed, the turbulence intensity is 0.1% in the inviscid core of the test section, away from the walls.

The (mechanical) wake was produced by placing a 25.4 mm diameter aluminum circular cylinder 50.8 mm from the start of the test section. The cylinder was oriented vertically and placed on the midplane of the tunnel. The thermal wake was generated by means of a mandoline. (The mandoline was developed by Warhaft and Lumley⁹ and consists of an array of fine, parallel, heated wires downstream of and oriented parallel to the cylinder. See Fig. 1 for a schematic.) It is constructed from 0.127 mm diameter wires that are heated using a variable DC power supply rated at 75 V and 15 A, maximum. The output voltage of the power supply is regulated to within 0.01%. Small springs are attached to the ends of the wires to prevent sagging, given that they expand when heated. The wires are attached to the wind tunnel walls by two end mounts that are electrically and thermally insulated by small ceramic plates. To obtain the best signal-to-noise ratio, the mandoline is operated at maximum power. This power depends on the resistance of the mandoline, which in turn depends on the number of wires (6–16) that compose the mandoline. As a result, two wire materials were used: (i) nichrome (type A) for mandolines consisting of more than 15 wires and (ii) stainless steel with an enamel coating for the remaining mandolines. The diameter of the wires (0.127 mm) was chosen such that it provided an acceptable tensile

strength, but was small enough to prevent the shedding of vortices ($Re_d = \langle U \rangle d_{wire} / \nu_{eff} < 40$) and therefore have negligible influence on the flow. (ν_{eff} is the kinematic viscosity evaluated at the film temperature [$T_{film} \equiv 1/2(T_{wire} + T_{\infty})$].) Beaulac³⁹ showed that the presence of the mandoline on the flow was small.

The longitudinal and transverse velocity components were measured using a TSI IFA 300 constant temperature hot-wire anemometer (operated at an overheat ratio of 1.8) in conjunction with a TSI 1241 X-wire probe. The hot wires were made of 3.05 μm diameter tungsten wires with a copper coating. (The copper coating is etched away using nitric acid to reveal the sensing portion of the wire.) The length-to-diameter ratio of the wires was ≈ 200 and they were separated by 1 mm. The X-wires are calibrated according to the effective angle technique proposed by Browne, Antonia, and Chua.⁴² Compensation of the velocity measurements for the variable temperature of the flow was performed by a modified King's law with temperature-dependent coefficients.⁴³

The temperature field was measured using a cold-wire thermometer built at the Université Laval (Québec, Canada) and based on a constant-current anemometer circuit.^{44,45} The probe current through the cold-wire sensors was 150 μA . The cold-wires were made from Wollaston wire with a 0.63 μm diameter platinum core, soldered to a TSI 1210 single-wire probe, and placed 1 mm away from the X wire. The length-to-diameter ratio of the etched portion of the wires was ≈ 800 [i.e., $l_{wire} \approx 0.5 \text{ mm}$ or $l_{wire} / \eta \approx 3$, where $\eta \equiv (\nu^3 / \epsilon)^{1/4}$ is the Kolmogorov microscale]. Given our interest in both large and small scales of the scalar field, this choice was a compromise between the competing effects of (i) spatial resolution and (ii) conduction between the cold wire and its prongs.⁴⁶ A complete discussion of this is given in Ref. 47.

The highest frequency in the flow f_{η} exceeds the frequency response of 0.63 μm diameter cold wires, as measured in Refs. 44, 48, and 49. For the flow velocities, Kolmogorov scales and wire diameters under consideration, it has been argued in Ref. 47 that the measurements are not seriously affected. Nevertheless, the present measurements were corrected for the finite cold-wire frequency response by a compensation technique proposed by Lemay and Benaïssa.⁴⁵ This method postprocesses the measured scalar time series in the frequency domain while modeling the frequency response of the cold-wire as a first-order linear system. Lastly, the cold-wire time constant and its corresponding cutoff frequency [τ_c and $f_c = 1/(2\pi\tau_c)$, respectively] were measured before each experiment using the current-injection technique described in Lemay and Benaïssa.⁴⁵ This method measures the response of the cold-wire to an injected square-wave current. From the wire response, τ_c can be determined, given the time constant of the electronics (see Lemay and Benaïssa⁴⁵). We found $\tau_c = 0.027 \text{ ms}$, which corresponds to $f_c = 5.9 \text{ kHz}$. The frequency response of the wire was measured before each experiment. If found to be abnormally slow (i.e., a drop in f_c —due to fouling, etc.—greater than or equal to 10% of its value when new), the cold wire was discarded and replaced with a new one.

The outputs of the hot-wire anemometer and the cold-

TABLE I. Flow parameters (at $x/D=53$). $D=0.0254$ m.

U_∞ (m/s)	10.2
$U_{centerline}$ (m/s)	8.8
ν (m^2/s)	16.0×10^{-6}
κ (m^2/s)	22.5×10^{-6}
$\langle u^2 \rangle$ (m^2/s^2)	0.375
$\langle \epsilon \rangle [= 15\nu/U^2 \langle (\partial u/\partial t)^2 \rangle]$ (m^2/s^3)	7.24
ℓ (m)	0.040
$Re_D (= U_\infty D/\nu)$	1.62×10^4
$R_\lambda (= \langle u^2 \rangle [15/(\nu\epsilon)]^{1/2})$	135
$R_\ell (= u_{rms}\ell/\nu)$	1531
$\eta [= (\nu^3/\epsilon)^{1/4}]$ (mm)	0.15
$\eta_\theta [= (\kappa^3/\epsilon)^{1/4}]$ (mm)	0.20

wire thermometer were both high- and low-pass filtered (using Kron-Hite 3382 and 3384 bandpass filters). The analog signals were subsequently digitized by means of a National Instruments PC-MIO-16E4 data acquisition board that was controlled using LABVIEW. Two types of data files were recorded. Data sets used in the calculation of time series, spectra, and longitudinal autocorrelations were sampled at twice the low-pass filter frequency (which was set to a frequency slightly larger than the Kolmogorov frequency). These sets consisted of 4.096×10^6 samples for centerline measurements. For off-centerline measurements, 4.096×10^5 samples were recorded. (All the measurements herein, with the exception of the transverse scalar autocorrelations, were made at the centerline.) Wyngaard's corrections for spatial resolution error^{50,51} were applied to the spectra. Data used to compute means and variances were sampled at a frequency roughly equal to the inverse of the integral time scale. These sets consisted of 4.096×10^5 samples for centerline measurements and 4.096×10^4 samples for off-centerline measurements.

III. FLOW CHARACTERISTICS

The purpose of this section is to characterize the velocity and temperature fields in the present experiments. Table I lists the flow parameters. Further details can be found in Ref. 39.

Figure 2 plots the mean longitudinal velocity and mean temperature profiles across the wake at a downstream location of $x/D=53$. The solid lines represent the best-fit Gaussian profiles to the data. The half width of the hydrodynamic wake at this downstream position is $2.4D$ —a value that is consistent with the measurements of Kang and Meneveau³³ and Matsumura and Antonia³² that are performed at slightly higher and lower Reynolds numbers, respectively. The half width of the thermal wake was slightly larger ($3.1D$)—a result consistent with the results of Antonia and Browne³⁸ and Rehab *et al.*⁵² Both profiles were measured over a range of $7D$ in the spanwise direction and found to be independent of z/D in this range.

Figure 3 plots the power spectra of u and θ at $x/D=53$ and $y/D=0$. The spectra resolved all scales, were free of noise, and—like the mean profiles—were found to be independent of z/D .

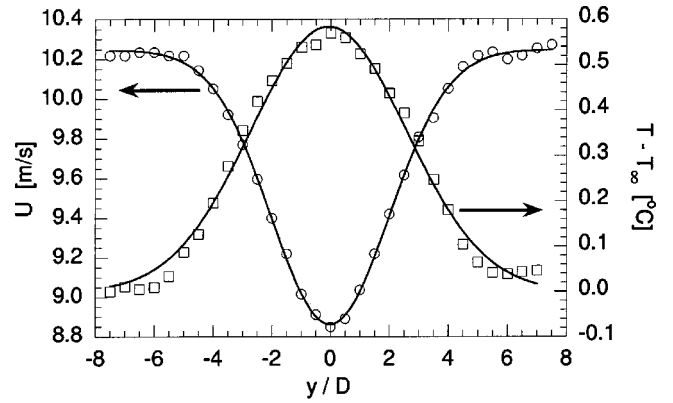


FIG. 2. The mean velocity and mean temperature profiles across the wake. \circ , U , left axis; \square , $T - T_\infty$, right axis. Solid lines are the best-fit Gaussian profiles. $x/D=53$. The mandoline used to generate the temperature profiles is located at $x_\theta/D=2$ and is composed of 11 wires, each separated by 2.54 mm (0.1 in.).

Finally, the passive nature of the scalar fluctuations was confirmed. Two types of tests were carried out: (i) tests comparing statistics of the velocity field in an isothermal wake to those in a heated wake and (ii) an estimation of the ratio of the integral scale ℓ to the Bolgiano length scale ($L_b \equiv \epsilon^{5/4} / [\epsilon_\theta^{3/4} (g\beta)^{3/2}]$), where β is the volumetric thermal expansion coefficient. (Calculation of this ratio is analogous to estimating the ratio of buoyant production of turbulent kinetic energy to its dissipation. Because the cylinder is vertical in our experiment, no mean temperature gradient exists in the direction of the gravitational vector and $g_i \theta u_i = 0$ by definition. It is for this reason that ℓ/L_b is calculated.) Differences in u_{rms} , ℓ , λ , η , ϵ , $S_u (\equiv \langle u^3 \rangle / \langle u^2 \rangle^{3/2})$, and $K_u (\equiv \langle u^4 \rangle / \langle u^2 \rangle^2)$ between the heated and unheated flow did not exceed 1.6%. The velocity spectra (of u and v) for the heated and unheated flows were the same at all scales (to within measurement error). The ratio ℓ/L_b was less than 2.5×10^{-6} at $x/D=89$ for the mandoline with the largest value of ϵ_θ . The passive nature of the scalar fluctuations is therefore clear. Such a result was expected given the small values of the temperature fluctuations in this flow.

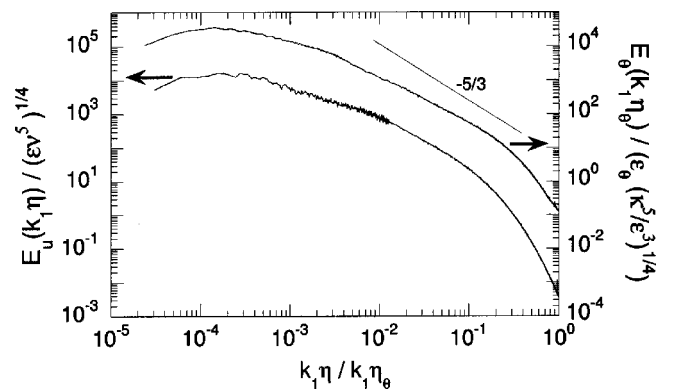


FIG. 3. The power spectra of longitudinal velocity and temperature at $x/D=53$ and $y/D=0$. (Velocity—lower curve, left axis; temperature—upper curve, right axis.) The mandoline used to generate the temperature profiles is located at $x_\theta/D=2$ and is composed of 11 wires, each separated by 2.54 mm (0.1 in.).

IV. RESULTS

The Lagrangian dispersion theory of Durbin,^{12,16} in conjunction with the experimental data of W&L and STH&C, have shown that, in grid-generated turbulence, the decay exponent of the scalar fluctuations (m) is principally determined by the ratio of the initial length scales of the velocity and temperature fields. In Sec. I, this parameter was expressed in terms of the ratio of the grid mesh length to the mandoline wire spacing (M/M_θ). Durbin¹² chose to express this parameter in terms of the velocity field integral length scale at the (scalar) injection point (ℓ_o) and the scalar injection scale L_θ . In the present work, this quantity will be called the *injection ratio* and denoted by ℓ_o/L_θ . Its relationship to the evolution of the scalar field in the turbulent wake of a cylinder will be studied herein.

ℓ_o is estimated by applying Taylor's hypothesis⁵³ and integrating the temporal autocorrelation of the longitudinal velocity fluctuations (along the centerline at $x=x_\theta$, the mandoline location) up to its first zero (e.g., Ref. 54, STH&C). The scalar field is created at x_θ and its integral length scale is not defined there. The scalar injection scale is therefore related to the geometry of the scalar injection mechanism—i.e., the mandoline width and wire spacing. To compare his theoretical work with the experiments of W&L and STH&C, Durbin¹² assumed $L_\theta=0.2M_\theta$. The appropriate definition of L_θ to use in this flow will be discussed in Sec. V. Lastly, note that the scalar injection scale differs from the integral scale of the scalar field (ℓ_θ).

W&L and STH&C varied the injection ratio by use of a mandoline in grid turbulence. They varied (i) ℓ_o by moving the mandoline downstream of the grid and (ii) L_θ by changing the mandoline wire spacing. In Sec. IV A, the effect of varying ℓ_o on the scalar field will be studied by moving a mandoline of fixed configuration downstream in the wake of a cylinder. In Sec. IV B the effect of varying L_θ on the scalar field will be examined by varying the mandoline configuration while keeping ℓ_o constant.

A. The effect of the velocity integral scale on the scalar field

In this section, the effect of the velocity field integral length scale is studied while keeping the mandoline configuration constant. The mandoline's width is set to the cylinder diameter ($w/D=1$) and is composed of 11 wires (i.e., $M_\theta/D=0.1$). This provides a good signal-to-noise ratio, while maintaining flow blockage effects to a minimum and is consistent with the experiments of L ev eque *et al.*⁴¹ The downstream evolution of the longitudinal integral length scales is shown in Fig. 4. One observes that ℓ increases as $(x/D)^{1/2}$, in accordance with the standard scaling arguments (e.g., Tennekes and Lumley⁵⁵). Given that ℓ_o is the (longitudinal) integral length scale measured along the centerline at $x=x_\theta$, a one-to-one relationship exists between x_θ/D , ℓ_o , and the injection ratio ℓ_o/L_θ (and increasing x_θ/D corresponds to increasing ℓ_o and ℓ_o/L_θ).

The analysis of Durbin¹² and the experiments of W&L and STH&C only study the range where the decay exponents of both velocity and temperature (n and m , respectively) are

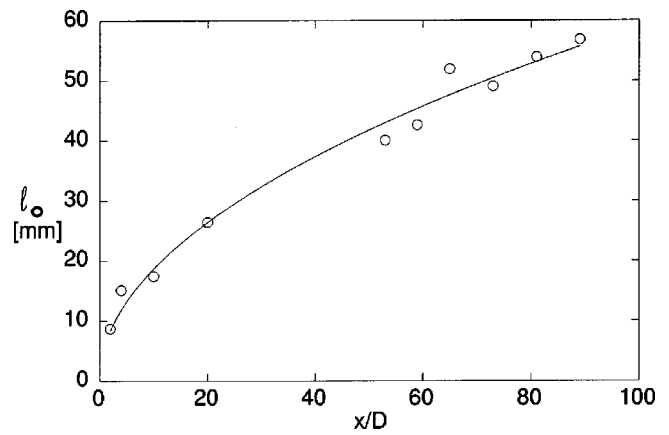


FIG. 4. Evolution of the integral length scale of u downstream of the cylinder. The solid line corresponds to $\ell=5.9(x/D)^{1/2}$.

constant. For the present flow, Beaulac³⁹ showed that the turbulent kinetic energy ($\frac{1}{2}\langle u_i u_i \rangle$) field follows a power-law dependence [given by Eq. (2)] for $x/D \geq 50$. He found the decay exponent n to be 0.72 (i.e., approximately half the value obtained in grid turbulence).⁵⁶ The explanation is presumably that, in the case of the wake, turbulent kinetic energy is produced by the mean velocity gradients and therefore reduces the decay rate of the fluctuating kinetic energy when compared to isotropic grid-generated turbulence (in which no production occurs). The value of the virtual origin is $x_o/D=30$. Given these observations, the decay rate of the scalar field is studied herein for $x/D \geq 50$ [viz., $53 \leq x/D \leq 89$, which corresponds to $23 \leq (x-x_o)/D \leq 59$].

Because (i) the objective of the present work is to study the effect of different physical parameters on the scalar decay rate in an inhomogeneous flow and (ii) Durbin¹² showed that m became independent of ℓ_o for $\ell_o/L_\theta \geq 2.5$, it is desirable to keep ℓ_o small to observe changes in the downstream evolution of the scalar field. This dictated x_θ/D , which varied from 2 to 20 in the present work. The effect of ℓ_o on the decay of the scalar field can be observed in Fig. 5, which

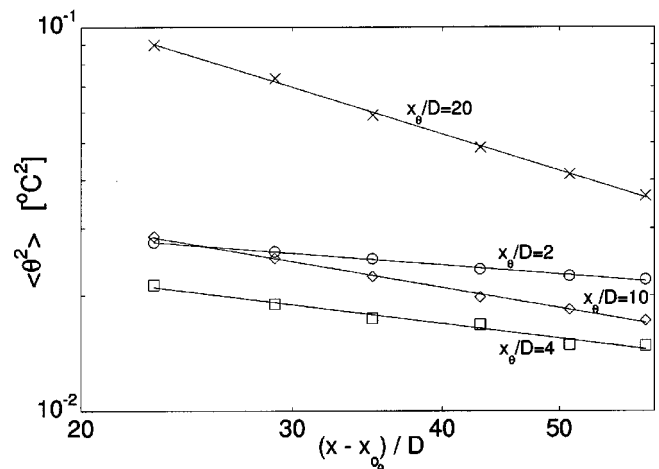


FIG. 5. The decay of the temperature variance as a function of mandoline downstream position. \circ , $x_\theta/D=2$; \square , $x_\theta/D=4$; \diamond , $x_\theta/D=10$; \times , $x_\theta/D=20$.

TABLE II. The effect of different mandoline locations on statistics pertaining to the scalar field. $w/D=1$, $M_\theta/D=0.1$. $\ell(x/D=53)=40$ mm; $\ell(x/D=89)=57$ mm. Note that A depends on the heating applied to the mandoline.

x_θ/D	A	m	ℓ_o (mm) [$=\ell(x_\theta/D)$]	$\ell_{\theta,x}$ (mm) [$x/D=53/89$]	$\ell/\ell_{\theta,x}$ [$x/D=53/89$]	r_{av}
2	0.060	0.25 ± 0.06	8.7	54/78	0.74/0.73	1.21
4	0.074	0.40 ± 0.06	15	45/61	0.89/0.93	1.27
10	0.159	0.55 ± 0.06	17	35/54	1.14/1.06	1.39
20	1.95	0.98 ± 0.04	26	23/38	1.74/1.50	1.80

plots the scalar variance⁵⁷ as a function of downstream distance for four different mandoline positions (x_θ/D). First, one observes that the data indeed follow a power-law decay of the form given by Eq. (1). Second, the decay exponents are found to be a (decreasing) function of x_θ/D , which implies a relationship between m and ℓ_o . These data are tabulated in Table II.

Note that in Fig. 5, x_{o_θ}/D was equal to 30 and was effectively independent of x_θ . Changing x_{o_θ} does change the value of m (which is determined by nonlinear least-squares regression). However, it was found that (i) the observed trends in m were independent of x_{o_θ} (i.e., the choice of virtual origin does not affect the relative rates of decay) and (ii) the observed variations in m over the small variations in x_{o_θ} ($30 \leq x_{o_\theta} \leq 35$) did not change any of our conclusions. Consequently, the virtual origin of the scalar (x_{o_θ}/D) was set to $30(=x_o/D)$.

Beaulac³⁹ showed that the statistics of the scalar field [e.g., its decay rate m , its skewness S_θ , its kurtosis K_θ , its probability density function PDF(θ), etc.] were independent of the heat input (and therefore the initial scalar fluctuation intensity). Because m is not a function of the heat input and only a function of ℓ_o , we consider their relationship. Figure 6 shows m plotted as a function of ℓ_o . It suggests that m increases with ℓ_o .

To relate m (and ℓ_o) to the structure of the scalar field, we next consider the (longitudinal) integral length scale of the scalar field, $\ell_{\theta,x}$. The longitudinal integral length scale of the scalar field is obtained by integrating the (longitudinal)

autocorrelation of θ up to its first zero. A variation in $\ell_{\theta,x}$ is clearly visible from Fig. 7, which plots the autocorrelation of θ at $x/D=53$ for the four mandoline locations under consideration. The scalar integral scale data corresponding to Fig. 7 (as well as data corresponding to $\ell_{\theta,x}$ at $x/D=89$) are also given in Table II. Therein, it is observed that $\ell_{\theta,x}$ decreases as x_θ/D increases—a result consistent with the notion that faster decay rates (larger m) are associated with smaller scales (smaller ℓ_θ).

Figure 8 substantiates this finding. Lumley and Panofsky⁵⁸ (p. 31) showed that the wavenumber corresponding to the peak of $k_1 E_\theta(k_1)$, k_{max} , is equal to the inverse of the integral length scale $\ell_{\theta,x}$ (assuming that the form of the autocorrelation is an exponential decay, which is a reasonable approximation for all but the smallest separations). $k_1 E_\theta(k_1)$ is plotted as a function of wavenumber in Fig. 8.⁵⁹ It is observed that the peak of these curves moves to larger wavenumbers as the mandoline is moved downstream. In other words, as ℓ_o increases, the scalar decay rate increases and the characteristic length of the scalar field decreases.

The decay exponent is plotted as a function of the peak wavenumber k_{max} in Fig. 9. Like in Fig. 16 of W&L (the equivalent figure for grid-generated turbulence),⁶¹ m appears to increase with k_{max} . W&L observed a close-to-linear relationship, which is not inconsistent with the present data. However, the relationship in both cases is not certain due to the lack of data.

As noted by W&L, turbulent flows should have time and length scale ratios that are connected to each other by the

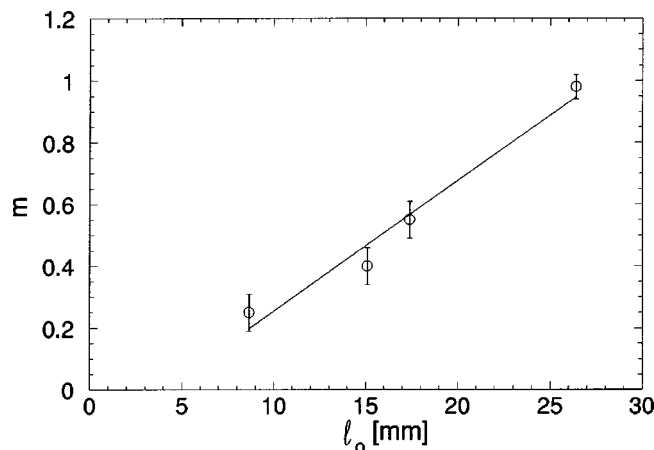


FIG. 6. The scalar decay rate exponent as a function of the velocity field integral scale measured at the scalar injection location.

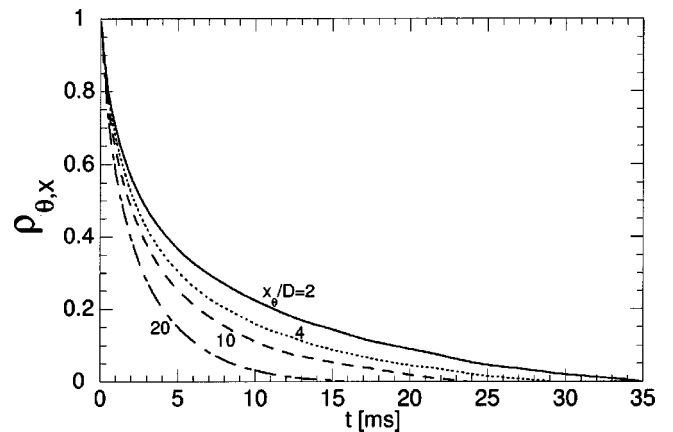


FIG. 7. Longitudinal autocorrelations of the scalar field for different mandoline locations. Solid line, $x_\theta/D=2$; short-dashed line, $x_\theta/D=4$; long-dashed line, $x_\theta/D=10$; dot-dash line, $x_\theta/D=20$. $x/D=53$.

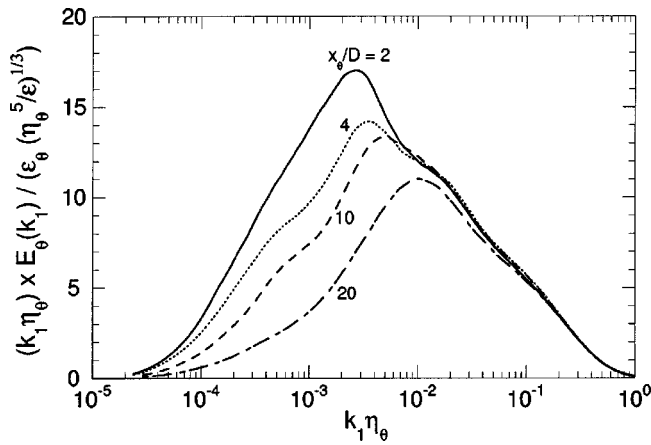


FIG. 8. Scalar spectra multiplied by the wavenumber for different mandoline downstream positions. Solid line, $x_\theta/D=2$; short-dashed line, $x_\theta/D=4$; long-dashed line, $x_\theta/D=10$; dot-dash line, $x_\theta/D=20$. $x/D=53$.

mean flow, i.e., faster time scales should be related to smaller length scales. We therefore study the ratio r of the mechanical to thermal time scales (τ and τ_θ), previously defined in Eq. (3). Recall that in grid-generated turbulence $r=m/n$ and given that n is constant, r and m have a linear, one-to-one relationship. However, in the present flow, $r \neq m/n$, due to the existence of turbulent transport and production in the scalar variance budget.

Using direct measurements [Eq. (3)], as well as indirect estimates by measuring the decay exponents of ϵ and ϵ_θ , Beaulac³⁹ verified that the time scale ratio r was a weak function of x/D . The latter estimates indicated that r should exhibit a decay exponent of 0.11–0.17. Such a slow evolution fell within the experimental scatter of the direct measurements and is consistent with W&L and STH&C. (Note that r is difficult to measure accurately. Béguier *et al.*,⁶² Sirivat and Warhaft,⁶³ and Zhou *et al.*⁶⁴ measured r the same way and obtained experimental error of the same magnitude.) Consequently, the (spatially) averaged time scale ratio r_{av} is defined as follows:

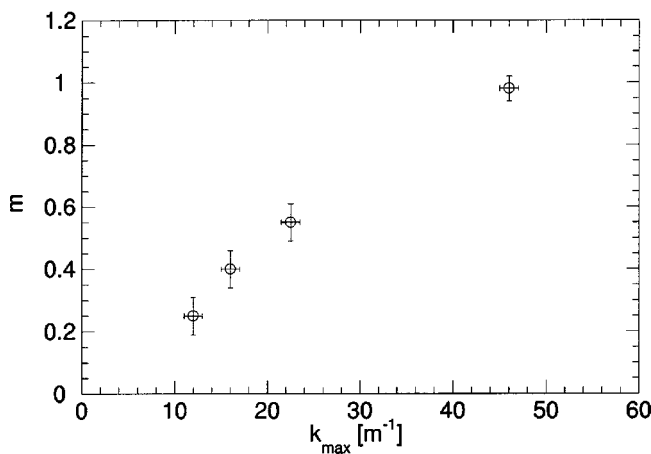


FIG. 9. The scalar decay exponent as a function of the wavenumber at the peak of $k_1 E_\theta$. $x/D=53$.

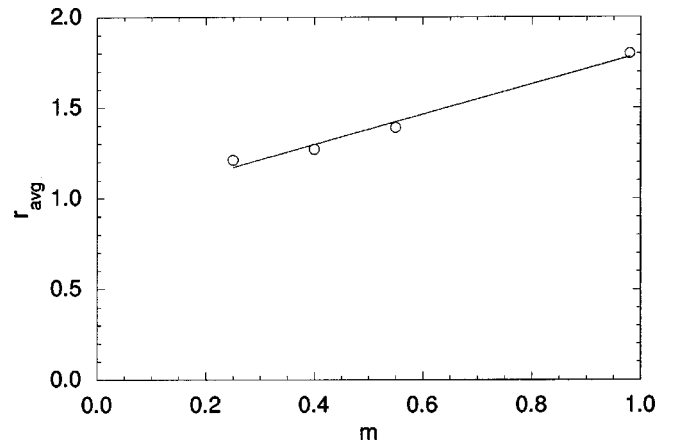


FIG. 10. The relationship between the mechanical to thermal time scale ratio and the scalar decay exponent.

$$r_{av} = \int_{53}^{89} r d(x/D). \tag{7}$$

Consideration of r_{av} should be satisfactory given that the decay exponent of r is at most half of the smallest value for m and can therefore be considered as evolving significantly more slowly than the scalar field itself. Values of r_{av} are compiled in Table II and range from 1.21 to 1.80. W&L observed values of r ranging from 0.6 to 2.4 while STH&C obtained $r=1.86$ for all their mandoline experiments. The relationship between r and m is plotted in Fig. 10. Given that (i) its ordinate is nonzero and (ii) its does not have a slope equal to $1/n=1/0.72 \approx 1.4$, it is clearly not of the form $r = m/n$.

To conclude the discussion of the effect of the velocity integral scale on the scalar field, we plot the time scale ratio as a function of the ratio of the integral scales of the velocity and thermal fields in Fig. 11. The observed increasing relationship is consistent with the notion that smaller length scales should have faster time scales.

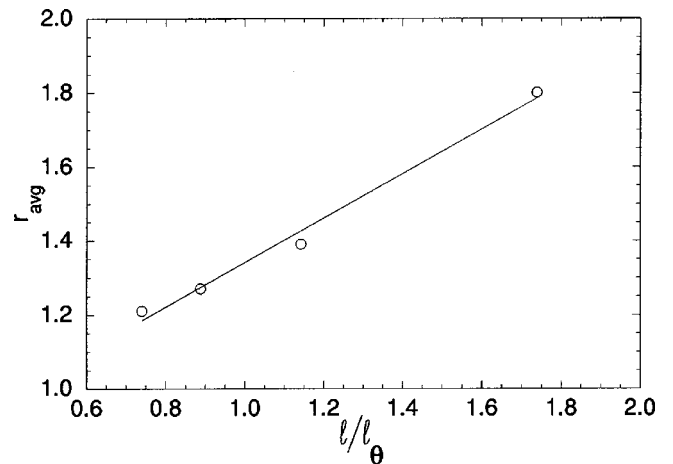


FIG. 11. The time scale ratio as a function of the ratio of the integral scales of the velocity and thermal fields.

TABLE III. The effect of different mandoline configurations on statistics pertaining to the scalar field. $\ell(x/D=53)=40$ mm; $\ell(x/D=89)=57$ mm. Note that A depends on the heating applied to the mandoline.

x_θ/D	w/D	M_θ/D	A	m	$\ell_{\theta,x}$ (mm) ($x/D=53/89$)	$\ell/\ell_{\theta,x}$ ($x/D=53/89$)	r_{av}
20	1	0.1	1.95	0.98 ± 0.04	23/38	1.74/1.50	1.80
20	2	0.4	0.16	0.76 ± 0.03	24/41	1.67/1.39	1.69
20	1	0.2	0.55	0.95 ± 0.02	23/40	1.74/1.43	1.75
20	2	0.2	0.82	0.77 ± 0.02	24/41	1.67/1.39	1.83
20	3	0.2	0.25	0.58 ± 0.04	24/41	1.67/1.39	1.68

B. The effect of the scalar injection scale on its field

In the preceding section that studied the effect of the velocity integral scale on the scalar field, the injection ratio ℓ_o/L_θ was varied by changing the integral length scale of the velocity field at the injection location (ℓ_o) while keeping the scalar injection scale (L_θ) constant. It was observed that—consistent with the experiments of W&L and the theory of Durbin¹²—increasing the injection ratio (ℓ_o/L_θ) increased the decay rate of the scalar field (m) and decreased the characteristic size of the scalar fluctuations ($\ell_{\theta,x}$ or k_{\max}^{-1}).

In the present section, we study the effect of the injection ratio on the scalar field by attempting to vary the scalar injection scale (L_θ) while keeping the integral length scale of the velocity field at the injection location (ℓ_o) constant.

W&L adjusted the scalar injection scale by varying the spacing between the mandoline wires (M_θ). Doing so, they observed changes in the scalar field and its decay rate. STH&C also varied the spacing between the wires of their heated screen, but the effect on the decay rate of the scalar variance was marginal because their wire spacings were too small compared to ℓ_o . That was not the case for W&L, where the different wire spacings were larger than the integral length scale of the velocity field.

Beaulac³⁹ attempted to independently vary L_θ in the present flow by changing M_θ . This, however, produced no significant changes. He found that halving or doubling M_θ had marginal effects on the scalar field and its downstream evolution (see Table III). Given that (i) ℓ is on the order of the wake width in the present flow and (ii) the (effective portion of the) mandoline can only be as wide as the width of the wake, it is impossible to have M_θ larger than ℓ_o . This can be interpreted as a similar result to that of STH&C, where M/M_θ ($\sim \ell_o/L_\theta$) took different values, all of which were, however, larger than unity. Therefore, a (potentially) different method of varying L_θ was sought out.

Another mandoline parameter exists in this flow with no fixed boundary that does not exist in homogeneous, isotropic turbulence: the mandoline width w . (The number of mandoline wires is not an independent parameter—it is uniquely determined by w and M_θ .) Its effect was therefore investigated (for widths where $w \geq \ell_o$, yet always contained within the fully turbulent region of the wake—see Beaulac³⁹). The three chosen widths were $w/D=1, 2$, and 3 . For these measurements, the mandoline wire spacing was constant ($M_\theta/D=0.2$) as was ℓ_o (by making all measurements at $x_\theta/D=20$).

Figure 12 shows the decay of the scalar variance for

mandolines of different widths. It can be observed that the data are well fitted by a power law and that the decay exponent m decreases as the mandoline width is increased. This behavior is consistent with the mandoline width w being a measure of the scalar injection scale L_θ and consequently agrees with Durbin's¹² theory, which suggests that m increases with the injection ratio ℓ_o/L_θ up to a critical value. (This will be further discussed in the following section.) The relationship between m and w is shown in Fig. 13. (Though only three data points appear in this figure, a linear relationship between m and w is also supported by measurements done with the mandoline located at other x_θ/D .)

It is clear that the width of the mandoline affects the downstream evolution of the scalar field. In the preceding section, such differences were associated with changes in the structure of the scalar field. It is therefore of interest to examine the characteristics of the scalar field when subjected to variations in w .

We begin by calculating the longitudinal, integral length scale of the scalar field $\ell_{\theta,x}$ at $x/D=53$. The longitudinal autocorrelation of θ for the three mandoline widths is shown in Fig. 14. Changing the mandoline width—and therefore the scalar injection scale—produces very small changes in the autocorrelation, indicating that $\ell_{\theta,x}$ is not affected by the width of the mandoline. The independence of $\ell_{\theta,x}$ to changes in w is also supported by the fact that the peak of $k_1 E_\theta$ is relatively insensitive to changes in w (Fig. 15).

Given that the wake is an inhomogeneous flow, longitudinal and transverse integral scales may be different.

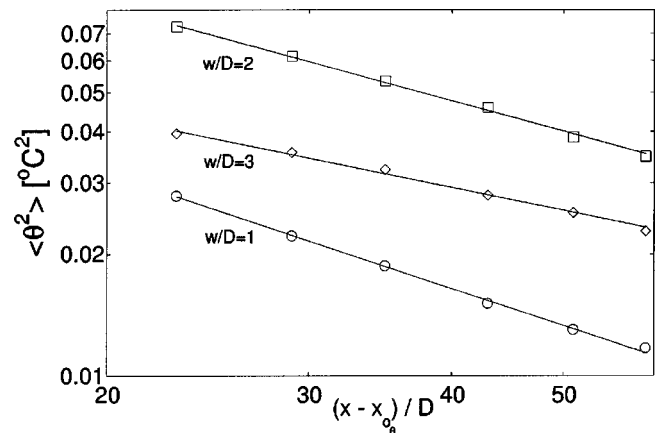


FIG. 12. The effect of w on the decay of $\langle \theta^2 \rangle$. \circ , $w/D=1$; \square , $w/D=2$; \diamond , $w/D=3$.

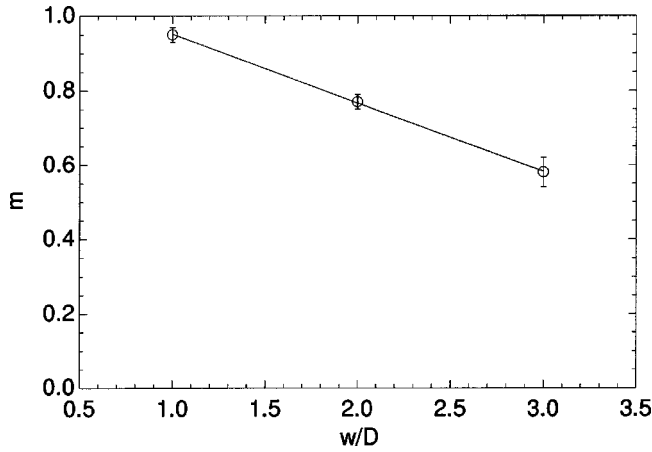


FIG. 13. The scalar decay rate as a function of the mandoline width.

Beaulac³⁹ measured the transverse autocorrelations of θ ($\ell_{\theta,y}$) using two cold wires separated in the transverse (y) direction and found (quantitatively and qualitatively) very similar results to those obtained with the longitudinal integral length scales. $\ell_{\theta,y}$ decreased as x_{θ}/D increased and it showed no significant dependence on w/D .

The fact that the downstream evolution of the scalar field can be modified without changing its structure is of significant interest. It is further studied by considering the mechanical to thermal time scale ratio r and how it reacts to changes in the width of the mandoline. For all three cases, r was again found to be weakly dependent on x/D , again supporting the use of r_{av} . (Its decay exponent was at most 0.13—less than one quarter of the smallest value of m for these experiments.)

The values obtained for r_{av} are 1.75, 1.83, and 1.68 for $w/D=1, 2,$ and $3,$ respectively. The variation of r_{av} is small and within the experimental scatter. There is, certainly, no trend in r_{av} with w like was observed with m . This may initially seem contradictory given that in previous work, the decay rate m and the time scale ratio r were directly linked due to the simplifications in the kinetic energy and scalar

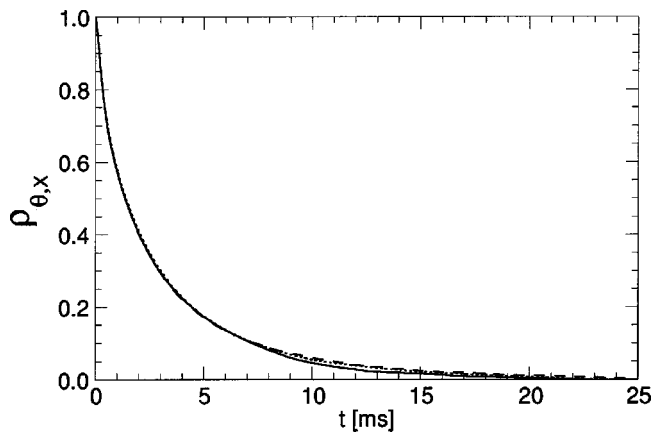


FIG. 14. Longitudinal autocorrelations of temperature for the three different mandoline widths. Solid line, $w/D=1$; short-dashed line, $w/D=2$; long-dashed line, $w/D=3$. $x/D=53$.

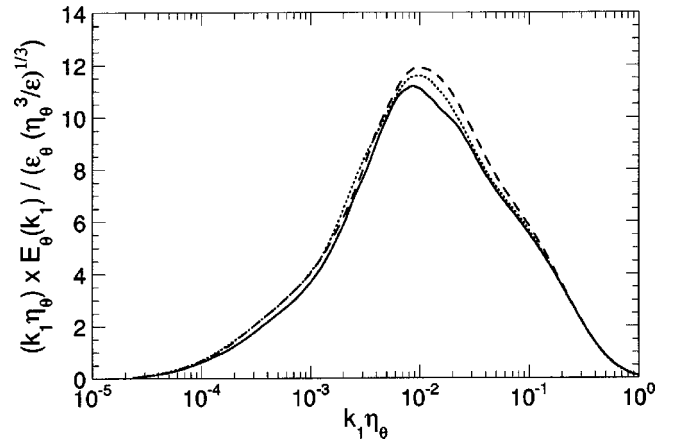


FIG. 15. Scalar spectra multiplied by the wavenumber for different mandoline widths. Solid line, $w/D=1$; short-dashed line, $w/D=2$; long-dashed line, $w/D=3$. $x/D=53$.

variance budgets. However, in the case of a turbulent wake, the turbulent transport and the mean scalar production terms play a capital role in decoupling r and m .

Lastly, as pointed out in the preceding section, r_{av} should be proportional to ℓ/ℓ_{θ} since shorter time scales are associated with smaller length scales. This still remains true in this section, because both r and ℓ_{θ} are independent of w/D and M_{θ}/D (and therefore L_{θ} —see Table III).

V. DISCUSSION

We begin by remarking that changing the mandoline position x_{θ} and geometry (i.e., L_{θ}) in the present experiments can be interpreted as independently varying different initial conditions of the scalar field. First, changing the mandoline geometry has no effect on the velocity field. However, doing so influences the scalar field. Therefore, varying the mandoline geometry and varying L_{θ} are directly related. Second, changing x_{θ} undoubtedly changes the velocity field integral scale at the injection point (ℓ_o). Doing so may also modify the one scalar field initial condition that may change when varying x_{θ} —namely, L_{θ}/W , where W is a length scale representative of the width of the wake. (An appropriate choice for W might be the wake half width.) However, the results of Sec. IV B of the paper clearly show that the *structure* of the scalar field is independent of L_{θ} (though not the scalar field's decay rate). Therefore, even though changing x_{θ} may modify a scalar field initial condition, the latter has no effect in this inhomogeneous flow. Consequently, the two sets of experiments performed in Secs. IV A and IV B vary different scalar field parameters independently.

It is also of interest to give a physical interpretation of our results. m decreased with increasing w or decreasing x_{θ} . Given a wider thermal wake (i.e., larger w), it will take the cold air outside of the wake longer to mix with the hotter air at its center. This will consequently retard the decay of the scalar fluctuations and result in a smaller m . In a similar fashion, decreasing x_{θ} (and therefore ℓ_o) given a fixed w will reduce the characteristic size of the velocity fluctuations with respect to the mandoline width. Consequently, the hot and cold air will not mix as rapidly and m will again be smaller.

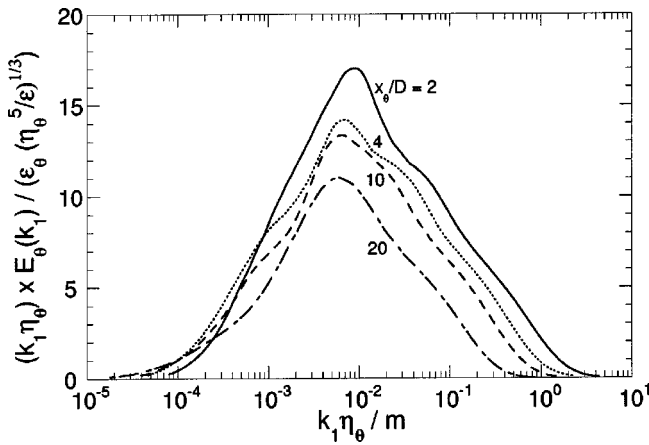


FIG. 16. The scalar spectrum multiplied by the wavenumber plotted as a function of $k_1 \eta_\theta / m$ for different mandoline downstream positions. Solid line, $x_\theta / D = 2$; short-dashed line, $x_\theta / D = 4$; long-dashed line, $x_\theta / D = 10$; dot-dash line, $x_\theta / D = 20$. $x / D = 53$.

We now proceed with a comparison of the results of the preceding section with the experiments of W&L and STH&C. Given that both previous works were undertaken in homogeneous, isotropic, grid-generated turbulence, the comparison should offer insight into the differences between homogeneous and inhomogeneous flows. In addition, it is tempting to interpret the previous results within the context of Durbin's theory,¹² even though it is not formally applicable to the present inhomogeneous, anisotropic flow. (Consequently, any observed differences cannot be interpreted as criticisms of the theory.)

The interpretation of the results of Sec. IV A are relatively straightforward and agree with the work of W&L and Durbin¹² in homogeneous, isotropic turbulence. Increasing x_θ / D causes ℓ_o , and consequently the injection ratio ℓ_o / L_θ to increase. This accelerates the decay of the scalar variance, as it did in W&L and as predicted by Durbin.¹² Similarly to W&L, the faster decay was accompanied by a decrease in the characteristic scale of the scalar field.

In their Figs. 20 and 21, W&L align the peak of their spectra by normalizing the abscissa (wavenumber) by r . In the present work, such a normalization did not align the peaks of the spectra, yet a normalization by m was successful in doing so. Figure 16 plots $k_1 E_\theta(k_1)$ as a function of the (nondimensional) wavenumber, normalized by m . Though the rationale behind such a normalization is not as evident as a normalization by r , the peaks appear to align. (The $x_\theta / D = 2$ case is the least aligned. It, however, is the case with the smallest value of m and therefore the largest relative error in its estimate.) Given that $r = m/n$ in the experiments of W&L, the present results are consistent with their Figs. 20 and 21. Nevertheless, the effect of the decoupling between r and m is clear in other results of Sec. IV.

The results of Sec. IV B are qualitatively different to those of Sec. IV A and can be viewed as having two interpretations—one that is based on the premise that $L_\theta \sim M_\theta$ and the other that is based on the premise that $L_\theta \sim w$.

In the first case, the independence of m on M_θ is—in

part—consistent with the work of STH&C and Durbin.¹² If the scalar injection scale L_θ in this flow is proportional to M_θ , then variations in the wire spacing should not result in changes in m or ℓ_θ , because $M_\theta \ll \ell_o$. This was observed to be the case. If $L_\theta \sim M_\theta$, changing the mandoline width while keeping M_θ constant should, in principle, not cause changes in m . The opposite was, however, observed in Sec. IV B and is inconsistent with work of STH&C and Durbin.¹²

The second premise ($L_\theta \sim w$) also gives results that are partially consistent with the work of Durbin¹² in as much as m increases with ℓ_o / L_θ . To further establish the applicability of Durbin's theory¹² to the present flow given this premise, it would be of interest to extend the present results to even larger injection ratios to observe whether the dependence of m on $L_\theta \sim w$ disappears for large ℓ_o / L_θ .

What is inconsistent in both cases is the observed variation in m without a corresponding variation in the structure of the thermal field (i.e., without observing corresponding changes in r , $\ell_{\theta x}$, $\ell_{\theta y}$, or k_{\max}^{-1}). This may result from the inhomogeneous nature of the flow and the consequently more complex relationship between the time scale ratio and the budgets of scalar variance and turbulent kinetic energy. The results of Sec. IV B indicate that the downstream evolution of the scalar field can be modified without changing its structure. Such a result may be of practical interest to the wide variety of industrial and environmental flows—which are generally inhomogeneous—given that it can be employed to enhance or inhibit the scalar mixing process, as desired.

Finally, because ℓ_θ is independent of the width of the mandoline, it is independent of the number of thermal sources in the wake. It would therefore be reasonable to extrapolate that a mandoline of only one wire (i.e., a single line source) would produce the same ℓ_θ . This hypothesis is possible given the linearity (in θ) of the equation governing the passive scalar field. Alternately stated, ℓ_θ should not be affected by the superposition of the other plumes onto the same velocity field. Validation of this hypothesis by measurements of the scalar field generated by a single line source would be beneficial and is planned.

VI. CONCLUSIONS

The downstream evolution of a scalar field was studied in an inhomogeneous flow—the turbulent wake of a circular cylinder. The scalar was injected by means of a mandoline, which enabled the variation of the scalar field initial conditions. Far enough away from the cylinder, the evolution of both the velocity and scalar fields followed a power-law behavior.

The response of the scalar field to changes in the integral scale of the velocity field at the injection point (ℓ_o) was similar to what has been observed in grid-generated turbulence—as ℓ_o was increased, the decay exponent of the scalar field (m) increased, the scalar field integral scale ℓ_θ decreased and the time scale ratio r increased. The peaks of $k_1 E_\theta$ do not collapse when the x axis is normalized by r , but do when normalized by m .

The response of the scalar field to changes in the scalar injection scale was more complex. In this flow, changing the

mandoline wire spacing M_θ , which—by necessity in this type of flow—was smaller than the integral scale of the velocity field at the mandoline location (ℓ_o), resulted in no significant changes in the structure (r , ℓ_θ , or k_{\max}^{-1}) or evolution (m) of the scalar field. If one assumes $L_\theta \sim M_\theta$, then this result is consistent with the work of STH&C and Durbin¹² who showed that for large enough values of the injection ratio, m lost its dependence on ℓ_o/L_θ .

Though the scalar field was not dependent on M_θ , it was shown to exhibit a clear dependence on the width of the mandoline w . Increasing the mandoline width caused the decay exponent m to decrease. This result is consistent with Durbin's theory,¹² if one assumes $L_\theta \sim w$. Changing w , however, had no significant effect on the structure of the scalar field (i.e., ℓ_{θ_x} , ℓ_{θ_y} , or k_{\max}^{-1}), nor did it affect the mechanical to thermal time scale ratio r . This result is of particular interest because it shows that the downstream evolution of the scalar field can be modified without changing the structure of the flow.

Lastly, the independence of m and r in this inhomogeneous flow is what, in a sense, "permits" the possibility of changing the downstream evolution of the scalar field without any modification of its structure. In homogeneous, isotropic flows, r and m are directly related to one another ($r = m/n$). However, this is not the case in inhomogeneous flows. Such a result can possibly be put to practical use in the wide variety of industrial, inhomogeneous flows (e.g., jets, wakes, etc.) to accelerate or decelerate the scalar mixing process, as desired.

ACKNOWLEDGMENTS

We thank E. Villermaux and Z. Warhaft for stimulating discussions. The work was funded by the Natural Sciences and Engineering Research Council of Canada and the Fonds pour la Formation de Chercheurs et l'Aide à la Recherche du Québec. In addition, S.B. was supported by means of a Natural Sciences and Engineering Research Council of Canada PostGraduate Scholarship.

- ¹Z. Warhaft, "Passive scalars in turbulent flows," *Annu. Rev. Fluid Mech.* **32**, 203 (2000).
- ²B. I. Shraiman and E. D. Siggia, "Scalar turbulence," *Nature (London)* **405**, 639 (2000).
- ³A. L. Kister, V. O'Brien, and S. Corrsin, NACA Report No. RM 54D19, 1954.
- ⁴A. L. Kister, V. O'Brien, and S. Corrsin, "Double and triple correlations behind a heated grid," *J. Aeronaut. Sci.* **23**, 96 (1956).
- ⁵R. R. Mills, A. L. Kister, V. O'Brien, and S. Corrsin, NACA Technical Report No. 4288, 1958.
- ⁶C. H. Gibson and W. H. Schwarz, "The universal equilibrium spectra of turbulent velocity and scalar fields," *J. Fluid Mech.* **16**, 365 (1963).
- ⁷T. T. Yeh and C. W. Van Atta, "Spectral transfer of scalar and velocity fields in heated-grid turbulence," *J. Fluid Mech.* **58**, 233 (1973).
- ⁸P. Sepri, "Two-point turbulence measurements downstream of a heated grid," *Phys. Fluids* **19**, 1876 (1976).
- ⁹Z. Warhaft and J. L. Lumley, "An experimental study of the decay of temperature fluctuations in grid-generated turbulence," *J. Fluid Mech.* **88**, 659 (1978).
- ¹⁰K. R. Sreenivasan, S. Tavoularis, R. Henry, and S. Corrsin, "Temperature fluctuations and scales in grid-generated turbulence," *J. Fluid Mech.* **100**, 597 (1980).
- ¹¹M. S. Mohamed and J. C. LaRue, "The decay power-law in grid-generated turbulence," *J. Fluid Mech.* **219**, 195 (1990).

- ¹²P. A. Durbin, "Analysis of the decay of temperature fluctuations in isotropic turbulence," *Phys. Fluids* **25**, 1328 (1982).
- ¹³G. R. Newman, B. E. Launder, and J. L. Lumley, "Modelling the behaviour of homogeneous scalar turbulence," *J. Fluid Mech.* **111**, 217 (1981).
- ¹⁴S. B. Pope, "PDF methods for turbulent reactive flows," *Prog. Energy Combust. Sci.* **11**, 119 (1985).
- ¹⁵S. B. Pope, *Turbulent Flows* (Cambridge University Press, Cambridge, 2000).
- ¹⁶P. A. Durbin, "A stochastic mode of two-particle dispersion and concentration fluctuations in homogeneous turbulence," *J. Fluid Mech.* **100**, 279 (1980).
- ¹⁷Z. Warhaft, "An experimental study of the effect of uniform strain on thermal fluctuations in grid-generated turbulence," *J. Fluid Mech.* **99**, 545 (1980).
- ¹⁸Z. Warhaft, "The use of dual heat injection to infer scalar covariance decay in grid turbulence," *J. Fluid Mech.* **104**, 93 (1981).
- ¹⁹Z. Warhaft, "The interference of thermal fields from line sources in grid turbulence," *J. Fluid Mech.* **144**, 363 (1984).
- ²⁰V. Eswaran and S. B. Pope, "Direct numerical simulations of the turbulent mixing of a passive scalar," *Phys. Fluids* **31**, 506 (1988).
- ²¹J. Lewalle, "Decay of velocity and temperature fluctuations in grid turbulence," *AIAA J.* **28**, 106 (1990).
- ²²D. J. Thomson, "A stochastic model for the motion of particle pairs in isotropic high-Reynolds-number turbulence, and its application to the problem of concentration variance," *J. Fluid Mech.* **210**, 113 (1990).
- ²³W. E. Mell, G. Kosaly, and J. J. Riley, "The length-scale dependence of scalar mixing," *Phys. Fluids A* **3**, 2474 (1991).
- ²⁴T. L. Jiang and E. E. O'Brien, "Simulation of scalar mixing by stationary isotropic turbulence," *Phys. Fluids A* **3**, 1612 (1991).
- ²⁵A. Junega and S. B. Pope, "A DNS study of turbulent mixing of two passive scalars," *Phys. Fluids* **8**, 2161 (1996).
- ²⁶M. S. Borgas and B. L. Sawford, "Molecular diffusion and viscous effects on concentration statistics in grid turbulence," *J. Fluid Mech.* **324**, 25 (1996).
- ²⁷M. Gonzalez and A. Fall, "The approach to self-preservation of scalar fluctuation decay in isotropic turbulence," *Phys. Fluids* **10**, 654 (1998).
- ²⁸T. Zhou, R. A. Antonia, L. Danaila, and F. Anselmetti, "Transport equations for the mean energy and temperature dissipation rates in grid turbulence," *Exp. Fluids* **28**, 143 (2000).
- ²⁹D. J. Thomson, "Dispersion of particle pairs and decay of scalar fields in isotropic turbulence," *Phys. Fluids* **15**, 801 (2003).
- ³⁰C. Tong and Z. Warhaft, "Passive scalar dispersion and mixing in a turbulent jet," *J. Fluid Mech.* **292**, 1 (1995).
- ³¹E. Villermaux, C. Innocenti, and J. Duplat, "Short circuits in the Corrsin–Obukhov cascade," *Phys. Fluids* **13**, 284 (2001).
- ³²M. Matsumura and R. A. Antonia, "Momentum and heat transport in the turbulent intermediate wake of a circular cylinder," *J. Fluid Mech.* **250**, 651 (1993).
- ³³S. H. Kang and C. Meneveau, "Passive scalar anisotropy in a heated turbulent wake: new observations and implications for large-eddy simulations," *J. Fluid Mech.* **442**, 161 (2001).
- ³⁴K. R. Sreenivasan, "Evolution of the centerline probability density function of temperature in a plane turbulent wake," *Phys. Fluids* **24**, 1232 (1981).
- ³⁵J. Mi and R. A. Antonia, "Evolution of centerline temperature skewness in a circular cylinder wake," *Int. Commun. Heat Mass Transfer* **26**, 45 (1999).
- ³⁶P. Freymuth and M. S. Uberoi, "Structure of temperature fluctuations in the turbulent wake behind a heated cylinder," *Phys. Fluids* **14**, 2574 (1971).
- ³⁷J. C. Larue and P. A. Libby, "Temperature and intermittency in the turbulent wake of a heated cylinder," *Phys. Fluids* **17**, 873 (1974).
- ³⁸R. A. Antonia and L. W. B. Browne, "Anisotropy of the temperature dissipation in a turbulent wake," *J. Fluid Mech.* **163**, 393 (1986).
- ³⁹S. Beaulac, M.Eng. thesis, McGill University, 2003.
- ⁴⁰G. Ruiz-Chavarria, C. Beaudet, and S. Ciliberto, "Scaling laws and dissipation scale of a passive scalar in fully developed turbulence," *Physica D* **99**, 369 (1996).
- ⁴¹E. Lévêque, G. Ruiz-Chavarria, C. Beaudet, and S. Ciliberto, "Scaling laws for the turbulent mixing of a passive scalar in the wake of a cylinder," *Phys. Fluids* **11**, 1869 (1999).
- ⁴²L. W. B. Browne, R. A. Antonia, and L. P. Chua, "Calibration of X-probes for turbulent-flow measurements," *Exp. Fluids* **7**, 201 (1989).
- ⁴³J. H. Lienhard V, Ph.D. thesis, University of California, San Diego, 1988.

- ⁴⁴J. Lemay (private communication).
- ⁴⁵J. Lemay and A. Benaissa, "Improvement of cold-wire response for measurement of temperature dissipation," *Exp. Fluids* **31**, 347 (2001).
- ⁴⁶L. W. B. Browne and R. A. Antonia, "The effect of wire length on temperature statistics in a turbulent wake," *Exp. Fluids* **5**, 426 (1987).
- ⁴⁷L. Mydlarski and Z. Warhaft, "Passive scalar statistics in high-Péclet-number grid turbulence," *J. Fluid Mech.* **358**, 135 (1998).
- ⁴⁸R. A. Antonia, L. W. B. Browne, and A. J. Chambers, "Determination of time constants of cold wires," *Rev. Sci. Instrum.* **52**, 1382 (1981).
- ⁴⁹J. C. LaRue, T. Deaton, and C. H. Gibson, "Measurement of high-frequency turbulent temperature," *Rev. Sci. Instrum.* **46**, 757 (1975).
- ⁵⁰J. C. Wyngaard, "Measurements of small-scale turbulence structure with hot wires," *J. Sci. Instrum.* **1**, 1105 (1968).
- ⁵¹J. C. Wyngaard, "Spatial resolution of a resistance wire temperature sensor," *Phys. Fluids* **14**, 2052 (1971).
- ⁵²H. Rehab, R. A. Antonia, and L. Djenidi, "Streamwise evolution of a high-Schmidt number passive scalar in a turbulent plane wake," *Exp. Fluids* **31**, 186 (2001).
- ⁵³G. I. Taylor, "The spectrum of turbulence," *Proc. R. Soc. London, Ser. A* **164**, 476 (1938).
- ⁵⁴G. Comte-Bellot and S. Corrsin, "Simple Eulerian time correlation of full- and narrow-band velocity signals in grid-generated 'isotropic' turbulence," *J. Fluid Mech.* **48**, 273 (1971).
- ⁵⁵H. Tennekes and J. L. Lumley, *A First Course in Turbulence* (MIT Press, Cambridge, 1972).
- ⁵⁶The decay exponent of the longitudinal velocity variance ($\langle u^2 \rangle$) was 0.65.
- ⁵⁷The scalar variance is not normalized by ΔT^2 because the latter was not measured with sufficient accuracy. In a heated wake, ΔT^2 is a function of x/D and follows a power-law behavior. This function is independent of x_θ . Therefore, computing m based on $\langle \theta^2 \rangle$ alone will not affect the analysis.
- ⁵⁸J. L. Lumley and H. A. Panofsky, *The Structure of Atmospheric Turbulence* (Wiley, New York, 1964).
- ⁵⁹All compensated spectra were smoothed by applying a Stineman function (Ref. 60) to the data, which was subsequently weighted geometrically over the current point $\pm 10\%$ of the data range.
- ⁶⁰R. W. Stineman, "A consistently well-behaved method of interpolation," *Creative Computing* **6**, 54 (1980).
- ⁶¹W&L's plot is a function of the wavenumber corresponding to the peak of the three-dimensional temperature spectrum. Given the anisotropic nature of this flow, it is impossible to estimate the three-dimensional spectrum from the measured, one-dimensional spectrum. However, the interpretation of k_{\max} in both cases is the same—a measure of the characteristic scale of the scalar fluctuations.
- ⁶²C. Bégulier, I. Dekeyser, and B. E. Launder, "Ratio of scalar and velocity dissipation time scales in shear flow turbulence," *Phys. Fluids* **21**, 307 (1978).
- ⁶³A. Sirivat and Z. Warhaft, "The effect of a passive cross-stream temperature gradient on the evolution of temperature variance and heat flux in grid turbulence," *J. Fluid Mech.* **128**, 323 (1983).
- ⁶⁴T. Zhou, R. A. Antonia, L. Danaila, and F. Anselmetti, "Transport equations for the mean energy and temperature dissipation rates in grid turbulence," *Exp. Fluids* **28**, 143 (2000).